Fuel 407 (2026) 137466

Contents lists available at ScienceDirect

Fuel

journal homepage: www.elsevier.com/locate/jfue

Full length article

Machine learning-enabled uncertainty quantification for thermo-catalytic reactors: A study on fugitive methane oxidation in monolith reactors

Israfil Soyler[a,*], Cihat Emre Üstün[a], Amin Paykani[a], Xi Jiang[a], Nader Karimi[b]

[a] School of Engineering and Materials Science, Queen Mary University of London, London, E1 4NS, United Kingdom
[b] School of Engineering, University of Southampton, Southampton, SO16 7QF, United Kingdom

HIGHLIGHTS

- Novel PCE-ANN framework delivers real-time UQ for catalytic combustion.
- 1000x speedup with no loss of accuracy.
- Inlet temperature dominates uncertainty.
- Flow velocity, concentration & catalyst deactivation are secondary effects.
- High temperatures (>950 K) reduce uncertainty; higher velocity increases it.

ARTICLE INFO

Keywords:
Fugitive methane
Ultra-lean catalytic combustion
Uncertainty quantification
Polynomial-chaos expansion (PCE)
Machine learning (ANN)
Monolith reactors

ABSTRACT

Ultra-lean methane oxidation via catalytic combustion is critical for mitigating greenhouse gas emissions from fugitive methane sources. However, the catalytic oxidation process exhibits significant uncertainties that hinder its widespread implementation. To address this challenge, the present study develops a robust machine learning-based framework for quantifying combustion uncertainties, enabling more effective emission control strategies. The work presents a novel hybrid methodology integrating polynomial chaos expansion (PCE) with artificial neural networks (ANN), achieving real-time prediction of methane conversion rates and their uncertainties in monolith reactors. The machine learning model reduces computational time from hours to seconds while achieving excellent agreement with detailed 1D plug-flow reactor simulations. The investigation reveals that variations in methane concentration (0.2 %–1.3 %, ± 10 %), inlet temperature (800–1000 K, ± 2 %), and inlet velocity (0.8–1.2 m/s, ± 5 %) significantly influence conversion uncertainty, with inlet temperature identified as the dominant parameter ($C_V \approx 75$ %). Stability improves at elevated temperatures (>950 K) and lower flow velocities ($C_V \approx 10$ %) compared to higher velocities (C_V = 17 %–22 %). Additionally, catalyst deactivation, represented by reduced coating length, decreases methane conversion rates and increases uncertainty, with longer coatings providing greater stability at higher inlet temperatures. This work advances the fundamental understanding of uncertainty propagation in ultra-lean catalytic methane combustion and establishes a generalisable, computationally efficient PCE-ANN framework applicable to catalytic combustion of diverse fuels.

1. Introduction

Climate change, driven largely by greenhouse gas (GHG) emissions from human activities, is one of the most critical global challenges. Methane, CH_4, with a global warming potential 28–36 times higher than CO_2 over a 100-year period, has emerged as the second most significant anthropogenic GHG, contributing roughly 30 % to global temperature rise [1,2]. The energy sector is a major source of CH_4 emissions, with significant contributions from oil production (≈50 Mt), natural gas systems (≈30 Mt), and coal mining (≈40 Mt) annually [3]. In coal mining, ventilation air methane (VAM) which maintains CH_4 concentrations below 5 vol% for safety, accounts for over 70 % of mine CH_4 emissions, despite its low concentration (≤1.5 vol%, typically <0.5 vol%) [4]. Mitigating these ultra-lean CH_4 emissions remains challenging due to operational issues such as large air volumes, fluctuating concentrations,

* Corresponding author.
Email address: i.soyler@qmul.ac.uk (I. Soyler).

https://doi.org/10.1016/j.fuel.2025.137466
Received 28 July 2025; Received in revised form 31 October 2025; Accepted 8 November 2025
Available online 19 November 2025

Nomenclature

Latin Symbols

A	Arrhenius constant
ANNs	Artificial Neural Networks
C_k	PCE coefficients
C_V	Coefficient of variation
CMC	Catalytic methane combustion
CPU	Central processing unit
CSTR	Continuous stirred-tank reactor
d	Dimension
E_a	Activation energy for the reaction
GHG	Greenhouse gas
GPR	Gaussian Process Regression
GWP	Global warming potential
HPC	High performance computing
IDT	Ignition delay time
LU	Legendre-Uniform distribution
MAE	Mean Absolute Error
MC	Monte Carlo
ML	Machine learning
NISP	Non-intrusive spectral projection
NNs	Neural Networks
n	Temperature exponent
N_{ord}	Parameter used for quadrature point generation
OP	Orthogonal polynomials
P	Total order
PCE	Polynomial chaos expansion
Pd	Palladium
PDF	Probability Density Function
PFR	Plug-flow reactor
Pt	Platinum
R	Universal gas constant
R^2	Coefficient of determination
R_c	Reactor catalyst coated length
ReLU	Rectified Linear Unit
S_i	Main sensitivity of a fuel composition
S_L	Laminar flame speed
SFR	Stagnation-flow reactor
T_{in}	Inlet temperature
UQ	Uncertainty quantification
UQTk	Uncertainty Quantification Toolkit
VAM	Ventilation air methane
Var[β]	Total variance of methane conversion
V_{in}	Inlet velocity

Greek Symbols

β_{CH_4}	Uncertainty associated with catalytic methane conversion rate
γ_θ	Relative uncertainty of input parameters
Γ	Catalyst surface site density
ϵ_i	Rate coefficient dependencies on the surface coverage
θ	Randomly sampled input parameters
Ψ_k	Multidimensional orthogonal polynomials
μ_i	Rate coefficient dependencies on the surface coverage
ξ	Quadrature points (germs)
π	Probability density function (PDF)
σ	Standard deviation
ϕ	Equivalence ratio

dust, and humidity [5]. Conventional combustion requires CH_4 concentrations within flammability limits (5 %–17 vol %) and risks producing NO_x emissions at high temperatures [6]. Catalytic methane combustion (CMC) offers a superior alternative by enabling CH_4 oxidation at concentrations well below the flammability limit and at significantly lower temperatures (as low as 400 °C), substantially reducing both GHG impact and NO_x formation [7]. The oxidation process of CMC converts CH_4 to CO_2, a far less potent GHG, reducing the climate impact substantially. Additionally, capturing CH_4 from VAM exhaust is more challenging than absorbing CO_2 [7]. Thus, converting fugitive CH_4 to low-GWP CO_2 in the energy sector supports climate change mitigation and improves air quality.

Noble metal catalysts, particularly platinum (Pt) and palladium (Pd) on Al_2O_3 supports, are widely used for CMC due to their high activity and low-temperature CH_4 conversion rates [7]. While Pd-based catalysts exhibit higher activity, Pt catalysts are preferred for ultra-lean CH_4 combustion due to better resistance to poisoning and lower costs [8,9]. Su and Yu [10] demonstrated this by developing a 25 kWe prototype using Pd/Al_2O_3 for lean CH_4 combustion from VAM systems. The prototype successfully operated with 0.8 % CH_4, generating 19–21 kWe without requiring cooling, air dilution, or nozzle injection. Burch et al. [11] compared Pt/Al_2O_3 and Pd/Al_2O_3 under various conditions, finding Pt superior in CH_4-rich environments and Pd more effective in O_2-rich (diluted) conditions. In addition to supported noble metals, recent reviews of Co_3O_4-based nanostructured catalysts, including noble metal doping strategies, have demonstrated the potential for enhanced catalytic performance and stability in lean methane combustion applications [12]. Furthermore, recent experimental studies on hierarchical monolith catalysts with self-supporting structures have demonstrated enhanced performance for lean methane catalytic oxidation [13].

Catalytic combustion in microreactors has gained attention due to their compact sub-millimetre-scale designs, offering advantages such as high surface-to-volume ratios, enhanced heat and mass transfer, and shorter diffusion times [9]. Honeycomb monolith reactors further improve performance with lower pressure drops, minimised external diffusion limitations, and prevention of hotspots due to their structured channels (round, square, or finned) [9]. These channels can be coated with thin, uniform catalyst layers, increasing fuel–catalyst contact area and enabling efficient use of noble metals. He et al. [14] experimentally investigated $Pt/\gamma\text{-}Al_2O_3$ catalysts in various microreactor channel types for CH_4 combustion. They tested Pt loadings (1.5–5.0 wt%), CH_4 flow rates (150-500 mL/min), O_2:CH_4 ratios (0.5–6.0), and temperatures (300–500 °C), finding that CH_4 conversion increases with Pt loading but decreases with higher flow rates, especially at higher loadings. The optimal O_2:CH_4 ratio was 1.5 (vs. the stoichiometric 2.0), balancing O_2 and CH_4 on the catalyst surface. The double serpentine channel design achieved the highest CH_4 conversion due to its larger coating area, longer residence time, and improved gas mixing. Hunt et al. [15] studied ultra-lean CH_4 combustion in a wavy channel microreactor with Pt catalyst, showing that strategic catalyst placement (using only 25 % of the coating) achieved 60 % of the CO_2 production of fully coated channels. The wavy design increased CO_2 production rates, per unit surface area of the catalyst, by up to 400 % compared to straight channels, highlighting the importance of channel configuration.

Dupont et al. [16] studied catalytic honeycomb monolith reactors with Pd and Pt catalysts for CH_4 combustion, highlighting their critical role in ignition and steady-state operation for complete CH_4 conversion to CO_2. They found that monolith length could be reduced by 70 % (from 50.8 mm) without performance loss, as the reaction zone is confined to the first 10–15 mm of the channels, offering significant cost savings in noble metal usage. Higher flow rates, however, pushed the reaction zone deeper into the monolith and reduced combustion stability [16]. Kumaresh et al. [17] numerically studied lean CH_4 combustion in Pt-coated honeycomb monoliths, showing complete CH_4 conversion

within 42 mm at 400 °C, 3 % fuel/air ratio, and 20 m/s inlet velocity. Higher inlet temperatures and fuel/air ratios, combined with lower velocities, shifted the reaction zone upstream, reducing the required reactor length. Deutschmann et al. [18] numerically investigated CH_4 combustion on Pt foil using a detailed surface reaction mechanism, successfully predicting complex phenomena like ignition, extinction, and hysteresis [18].

VAM systems face significant variability challenges due to ultra-lean CH_4 concentrations (0.1 %–1.5 %) and large ventilation air flows (100–300 m^3/s) [19]. These variations, caused by mining activities and underground pressure changes, affect gas quality, flow rate, and purity [4,19]. Rahimi et al. [20] emphasised designing ventilation systems to account for gas emission uncertainties, ensuring safety against fires, explosions, and financial losses from coal seam gas fluctuations. Combustion systems for VAM must handle these uncertainties, as sudden flow reductions disrupt combustion stability, while rapid CH_4 concentration increases risk equipment damage and higher NO_x emissions [9]. Additionally, low-concentration CH_4 often contains contaminants like dust, NO_x, H_2O, H_2S, and SO_2, which can poison and deactivate catalysts [9]. Catalyst deactivation in monolithic reactors remains a challenge due to uncontrolled emissions and incomplete combustion [21]. Temperature is critical, affecting reaction kinetics, catalyst activity, and stability. While catalytic combustion occurs at lower temperatures [7], precise temperature control is essential to avoid thermal stress, mechanical degradation, and accelerated deactivation [21,22]. Uncontrolled temperature variations, especially when using waste heat, further complicate system performance [23]. These operational challenges underscore the need for systematic approaches to quantify and manage uncertainty in catalytic fugitive methane combustion.

Although previous studies discussed the presence of uncertainty in VAM systems, there remains a significant gap in the literature regarding systematic uncertainty quantification (UQ) in catalytic ultra-lean CH_4 combustion applications. Both experimental and computational approaches inherently contain unavoidable uncertainties, while traditional numerical models employ fixed parameters [24]. These uncertainties can be effectively quantified and reduced through mathematical modelling techniques. Uncertainties generally fall into two categories: epistemic and aleatoric. Epistemic uncertainty stems from lack of knowledge or information about the system and can potentially be decreased through improved understanding and enhanced measurement techniques. Conversely, aleatoric uncertainty arises from the probabilistic nature of random processes and is irreducible, even with complete system knowledge [25]. In this study, the computational framework primarily focuses on epistemic uncertainty through the analysis of parametric variations in inlet conditions (temperature, velocity, and concentration) and catalyst coating length. These variations represent uncertainties that could theoretically be reduced with improved measurement, control systems, and catalyst design. By quantifying how these epistemic uncertainties propagate through the catalytic system, the parameters that contribute most significantly to variability in methane conversion performance can be identified. Uncertainty quantification methods use mathematical modelling to measure and manage uncertainties in experimental and computational settings [24,26,27]. While Monte Carlo (MC) methods traditionally address epistemic uncertainties, they are computationally expensive for complex models requiring large sample sizes [28]. Surrogate models, such as Gaussian processes [29,30] or Polynomial Chaos Expansion (PCE) [31,32], provide efficient alternatives to computationally expensive MC methods for UQ. For complex simulations, UQ-PCE is more cost-effective and efficient than UQ-MC; several studies have successfully applied PCE-based UQ methods to combustion problems [33–36].

While PCE significantly improves efficiency for UQ, it still remains demanding for complex catalytic systems requiring high-fidelity simulations with detailed chemistry and transport phenomena. Soyler et al. [36] demonstrated this computational burden by using PCE for UQ in $NH_3/H_2/N_2$/air combustion, completing over 21,000 simulations (6000 CPU hours) on an HPC cluster. In a follow-up study, they performed 70,000 simulations to analyse uncertainties in partially cracked NH_3/syngas combustion [37]. Similarly, Zhang and Jiang [31,38,39] demonstrated the need for extensive simulations in PCE-based UQ for combustion research. This computational burden presents a significant obstacle to the practical implementation of UQ for real-world catalytic applications, particularly for real-time monitoring and control systems necessitating more efficient approaches. The novel integration of machine learning (ML) with UQ techniques offers a promising solution to overcome this limitation by drastically reducing computational costs while maintaining accuracy [40], and enabling robust analysis of uncertainty propagation in catalytic methane combustion systems. ML techniques efficiently capture complex relationships between uncertain parameters and system outputs, enabling analysis of non-linearities and interactions without extensive model evaluations. Recent research has explored various ML algorithms for combustion properties, including laminar flame speed (S_L) [41,42], ignition delay time (IDT) [43], and reforming processes [44]. Among these approaches, artificial neural networks (ANNs) have proven their effectiveness in combustion applications and their ability to model highly non-linear relationships between multidimensional input and output spaces [45], making them especially suited for catalytic conversion processes where multiple interacting parameters influence reaction outcomes. ML-based UQ frameworks enable robust design and optimisation of catalytic reactors under varying conditions, making them particularly valuable for catalytic VAM systems, where real-time prediction and optimisation under uncertainty are critical for practical implementation.

To the best of authors' knowledge, no prior studies have explored ML-based UQ for catalytic combustion systems, revealing a significant research gap. While ML and UQ have been applied to combustion modelling, their integration for directly predicting uncertainty metrics in catalytic systems remains unexplored. This study addresses this gap by developing a novel ML framework to predict uncertainty bounds, sensitivity indices, and probabilistic performance metrics for catalytic CH_4 oxidation. The specific objectives of this work include several key components. First, an ML model (ANN) for predicting catalytic CH_4 conversion rates in monolith reactors is developed and validated. Second, the effects of varying CH_4 concentration, inlet temperature, and inlet flow velocity on uncertainty in CH_4 conversion are quantified using a surrogate UQ method (PCE). Third, the influence of catalyst deactivation on conversion performance and uncertainty propagation is investigated. Fourth, dominant parameters driving uncertainty in ultra-lean catalytic CH_4 combustion are identified. Finally, the computational efficiency of the PCE-ANN framework compared to conventional approaches is demonstrated.

Once trained, the ML model delivers a remarkable computational advantage, reducing analysis time from hours to seconds while preserving high-fidelity uncertainty predictions. This hybrid PCE-ANN approach advances catalytic systems modelling in two crucial dimensions: theoretically, by elucidating the nonlinear propagation mechanisms of parametric uncertainties through complex surface reactions; and practically, by providing rapid assessment tools essential for robust fugitive CH_4 oxidation technology design. By quantitatively mapping how input uncertainties transform into performance variability, this framework establishes science-based safety margins, optimise operating conditions, and implements targeted control strategies that maximise conversion reliability while minimising catalyst deactivation. The resulting decision support capability addresses a critical gap in the development of resilient catalytic combustion systems for GHG mitigation applications.

2. Methodology

2.1. Uncertainty quantification method

In this work, PCE was employed to construct a surrogate model for UQ using the open-source Uncertainty Quantification Toolkit (UQTk)

Table 1
Surface reaction mechanism for CH_4 combustion over Pt catalyst from Deutschmann et al. [50].

	Reaction	A (cm, mol, s)	n	E_a (kJ/mol)	ε_i, μ_i(kJ/mol)
(1)	H_2 + 2Pt(s) → 2 H(s)	4.60×10^{-2}			$\mu_{Pt(s)} = -1^*$
(2)	2 H(s) → H_2 + 2Pt(s)	3.70×10^{21}	0.0	67.4	$\varepsilon_{H(s)} = 6$
(3)	H + Pt(s) → H(s)	1.00^*			
(4)	O_2 + 2Pt(s) → 2O(s)	1.80×10^{21}	−0.5	0.0	
(5)	O_2 + 2Pt(s) → 2O(s)	$2.30 \times 10^{-2*}$			
(6)	2O(s) → 2Pt(s) + O_2	3.70×10^{21}	0.0	213.2	$\varepsilon_{O(s)} = 60$
(7)	O + Pt(s) → O(s)	1.00^*			
(8)	H_2O + Pt(s) → H_2O(s)	0.75^*			
(9)	H_2O(s) → H_2O + Pt(s)	1.00×10^{13}	0.0	40.3	
(10)	OH + Pt(s) → OH(s)	1.00^*			
(11)	OH(s) → OH + Pt(s)	1.00×10^{13}	0.0	192.8	
(12)	O(s) + H(s) → OH(s) + Pt(s)	3.70×10^{21}	0.0	11.5	
(13)	H(s) + OH(s) → H_2O(s) + Pt(s)	3.70×10^{21}	0.0	17.4	
(14)	OH(s) + OH(s) → H_2O(s) + O(s)	3.70×10^{21}	0.0	48.2	
(15)	CO + Pt(s) → CO(s)	$8.40 \times 10^{-1*}$			$\mu_{Pt(s)} = 1$
(16)	CO(s) → CO + Pt(s)	1.00×10^{13}	0.0	125.5	
(17)	CO_2(s) → CO_2 + Pt(s)	1.00×10^{13}	0.0	20.5	
(18)	CO(s) + O(s) → CO_2(s) + Pt(s)	3.70×10^{21}	0.0	105.0	
(19)	CH_4 + 2Pt(s) → CH_3(s) + H(s)	$1.00 \times 10^{-2*}$			$\mu_{Pt(s)} = 0.3$
(20)	CH_3(s) + Pt(s) → CH_2(s) + H(s)	3.70×10^{21}	0.0	20.0	
(21)	CH_2(s) + Pt(s) → CH(s) + H(s)	3.70×10^{21}	0.0	20.0	
(22)	CH(s) + Pt(s) → C(s) + H(s)	3.70×10^{21}	0.0	20.0	
(23)	C(s) + O(s) → CO(s) + Pt(s)	3.70×10^{21}	0.0	62.8	
(24)	CO(s) + Pt(s) → C(s) + O(s)	1.00×10^{18}	0.0	184.0	

$k = AT^n e^{(-E_a/RT)}$, k is the rate constant for the reaction, A is the Arrhenius constant, n is the temperature exponent,
E_a is the activation energy for the reaction, and R is the universal gas constant.
ε_i and μ_i are the rate coefficient dependences on the surface coverage.
* symbol represents the sticking coefficient.

version 3.1.4 [46]. The mathematical formulation of the PCE surrogate model is briefly described below. The uncertainty in simulation parameters is expressed as:

$$\theta_{\text{sample}} = \theta_{\text{mean}} \pm \sigma_\theta \times \xi_d \tag{1}$$

where θ_{sample} represents a randomly sampled set of parameters for catalytic CH_4 oxidation, such as inlet temperature (T_{in}), inlet velocity (V_{in}), or equivalence ratio (ϕ). The mean values of these parameters are denoted by θ_{mean}, and their standard deviations by σ_θ. The random variable germs, $\xi_d = (\xi_{T_{\text{in}}}, \xi_{V_{\text{in}}}, \xi_\phi)$, are generated using orthogonal polynomials based on the distribution type [47,48]. These germs represent the standardised basis for constructing PCE, where each element corresponds to a specific uncertain input parameter (inlet temperature, inlet velocity, and equivalence ratio, respectively). The orthogonal polynomials are selected to match the probability distribution of each parameter (Hermite polynomials for normal distributions and Legendre polynomials for uniform distributions), ensuring optimal convergence of the expansion. For this study, a Legendre-Uniform (LU) distribution was assumed, with random variables uniformly distributed in the interval $[-1, 1]$. The standard deviation of each parameter is calculated as follows:

$$\sigma_\theta = \theta_{\text{mean}} \times \gamma_\theta \tag{2}$$

where γ_θ represents the relative uncertainty: 5 % for inlet velocity ($\gamma_{V_{\text{in}}} = 0.05$), 10 % for equivalence ratio ($\gamma_\phi = 0.10$), and 2 % for inlet temperature ($\gamma_{T_{\text{in}}} = 0.02$).

The number of quadrature points (ξ_d) is calculated as $(N_{\text{ord}})^d$, where $N_{\text{ord}} = P + 1$ is the expansion order, and d is the number of uncertain parameters. With $P = 5$, this results in $(5 + 1)^3 = 216$ quadrature points. Higher-order expansions can lead to excessive quadrature points without improving UQ results [36]. The selection of $P = 5$ was based on the authors' previous implementation in similar combustion UQ studies [36,37], where they demonstrated that orders higher than $P = 5$ did not provide significant improvement in accuracy while substantially increasing computational cost. For this catalytic system with 3 uncertain parameters, $P = 5$ is sufficient to capture the output variance while maintaining computational load with 216 evaluation points per case.

The multidimensional PCE for catalytic CH_4 conversion is expressed as:

$$\beta_{\text{CH}_4} = \sum_{k=0}^{P} C_k \Psi_k(\xi_d) \tag{3}$$

where β_{CH_4} represents CH_4 conversion with quantified uncertainty, C_k are the PCE coefficients (spectral mode strengths), and $\Psi_k(\xi_d)$ are Legendre-Uniform orthogonal polynomials up to order P. The PCE coefficients are determined using the non-intrusive spectral projection (NISP) method via Gauss-Legendre quadrature integration:

$$C_k = \frac{1}{\langle \Psi_k^2(\xi) \rangle} \int_{-1}^{1} \beta(\xi) \Psi_k(\xi) \pi(\xi)\, d\xi, \quad k = 0, \ldots, P \tag{4}$$

where $\pi(\xi)$ is the probability density function, and ξ represents the germ samples for each input parameter.

In addition to quantifying uncertainties in CH_4 conversion, a variance-based global sensitivity analysis [49] was conducted to evaluate the impact of input uncertainties on output uncertainty. This method assesses how individual parameter uncertainties contribute to the total uncertainty in CH_4 conversion. The first-order sensitivity indices (S_i) are calculated as:

$$S_i = \frac{\sum C_i^2 \langle \Psi_i^2 \rangle}{\text{Var}[\beta]} \tag{5}$$

where (i) denotes a specific input parameter, and $\text{Var}[\beta]$ represents the total variance of CH_4 conversion. The total variance is expressed as:

$$\text{Var}[\beta] = \sum_{k>0} C_k^2 \langle \Psi_k^2 \rangle \tag{6}$$

2.2. Validation of surface reaction mechanism

The surface reaction mechanism developed by Deutschmann et al. [50] was used, comprising 24 chemical reactions involving 11 surface species and 7 gas-phase species (Table 1). Pt catalyst was modelled with

a surface site density (Γ) of 2.72×10^9 mol/cm^2, where Pt(s) represents uncovered surface sites available for adsorption.

The mechanism was validated using two models: a stagnation-flow reactor (SFR) and a plug-flow reactor (PFR). The SFR configuration, where gas flow impinges perpendicularly onto a catalytic surface, is ideal for studying gas-surface interactions and reaction kinetics. Its 1D nature simplifies analysis by focusing on the centreline, where variables depend only on the distance from the surface, making it suitable for validating detailed reaction mechanisms [18].

For catalytic CH_4 combustion simulations in a SFR, Cantera [51] was used to solve the surface chemistry reactions. The simulations were conducted under specified initial conditions to validate the surface reaction mechanism. A premixed gas mixture of 9.5 % CH_4 in air was introduced with a uniform inlet velocity of 6 cm/s at 100 mm from the catalytic surface. The initial CH_4-air mixture and surface temperatures were set to 300 K and 1000 K, respectively, under atmospheric pressure.

The surface reaction mechanism was validated against the results of Deutschmann et al. [18] using an SFR configuration. Fig. 1 compares species mole fractions as a function of distance from the catalytic surface. The continuous lines represent the current numerical results, while the marker points show data from Deutschmann et al. [18]. The simulation captures the key features of species evolution: O_2 and CH_4 are consumed near the surface, while CO_2 and H_2O are formed. A small amount of CO appears as an intermediate species, peaking near the surface before being oxidised to CO_2. The excellent agreement between the simulations and reference data validates the implementation of the surface reaction mechanism.

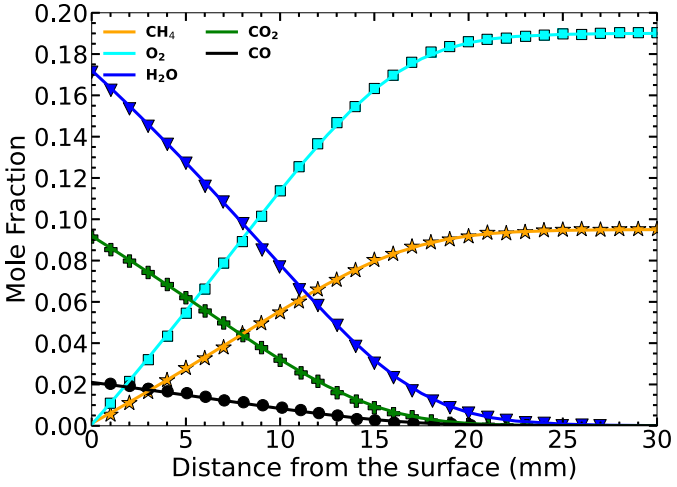

Fig. 1. Validation of surface reaction mechanism using SFR simulations. Continuous lines represent numerical results from this study, while markers denote reference data from Deutschmann et al. [18].

The PFR represents a steady-state 1D flow system where species concentrations and temperature vary along the reactor length without diffusion. In this model, the reaction mixture flows uniformly at constant velocity, ensuring complete radial mixing and no backflow. The PFR is particularly suitable for catalytic systems, as surface reactions at the wall promote radial mixing. Its computational efficiency makes it an excellent tool for validating detailed kinetic mechanisms under steady-state conditions.

In this work, catalytic CH_4 combustion simulations were performed in a single-channel PFR with a length of 200 mm and a hydraulic diameter of 1.27 mm. The reactor simulated lean premixed CH_4-air combustion over a Pt catalyst at atmospheric pressure. Cantera was used to model the PFR as a chain of 201 continuous stirred-tank reactors (CSTRs). The governing equations for the 1D steady-state PFR model are detailed elsewhere [51]. The first CSTR was fed a lean CH_4/air mixture (fuel/air ratio 2.94 %) at an inlet temperature of 645 °C and an inlet velocity of 16.7 m/s.

The surface reaction mechanism from Deutschmann et al. [50] was further validated against the results of Kumaresh and Kim [17] using a PFR configuration. Fig. 2 compares the current results (continuous lines) with data from Kumaresh and Kim [17] (marker points). Initially, the Pt surface is predominantly covered by adsorbed oxygen O(s), with a coverage of approximately 0.9 at the reactor entrance.

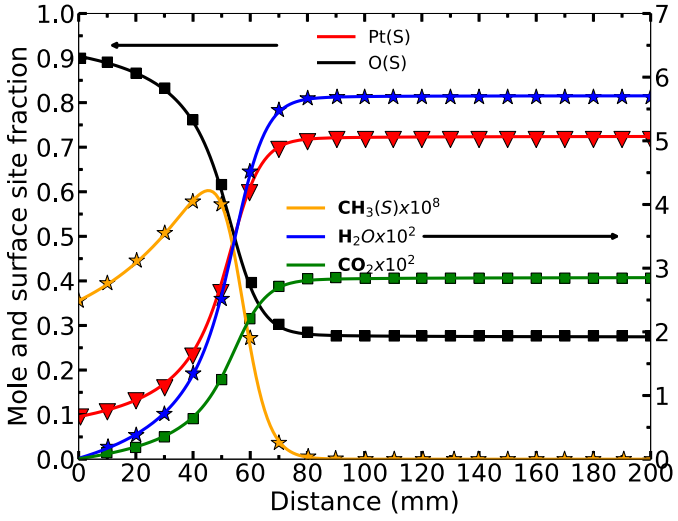

Fig. 2. Validation of Deutschmann's surface mechanism with the results from Kumaresh and Kim by using PFR reactor. Continuous lines are from this study, marker points are from Kumaresh and Kim [17].

As reactions proceed, O(s) coverage decreases while free Pt(s) increases, stabilising at about 0.7 after 60 mm. The adsorbed methyl species CH_3(s) (scaled by 10^8 for clarity) peaks at 40–50 mm, indicating the region of most active CH_4 decomposition, before being consumed in subsequent reactions. The formation of CO_2 and H_2O (scaled by 10^2 for clarity) increases until reaching steady-state values after about 80 mm. The excellent agreement between our simulations and the reference data validates both the surface mechanism implementation and the PFR model assumptions under the specified conditions.

2.3. Machine learning (ML)

In this work, ML models were developed to predict how variations in input parameters affect ultra-lean catalytic CH_4 conversion rates, efficiently capturing complex reaction behaviours under different operational conditions. This section describes the data generation process, including associated uncertainties for 1D simulations using Cantera, followed by an introduction to the ANN methodology. Fig. 3 presents a detailed overview of the PCE-ANN framework employed in this study, illustrating the integration of UQTk, Cantera, ANN development, and potential applications.

2.3.1. Data generation

Honeycomb monolith reactors are widely used for emission reduction due to their high surface area, low pressure drop, uniform flow distribution, thermal stability, durability, and versatility [52]. These reactors consist of numerous small-diameter channels coated with catalysts on their interior surfaces. In this work, a single channel is analysed, as each channel exhibits similar behaviour [50].

To train the ML models, operational input parameters with associated uncertainties were generated using UQTk software, and a comprehensive dataset was created through 1D simulations in Cantera [51]. The simulations focused on ultra-lean catalytic CH_4 combustion in a PFR,

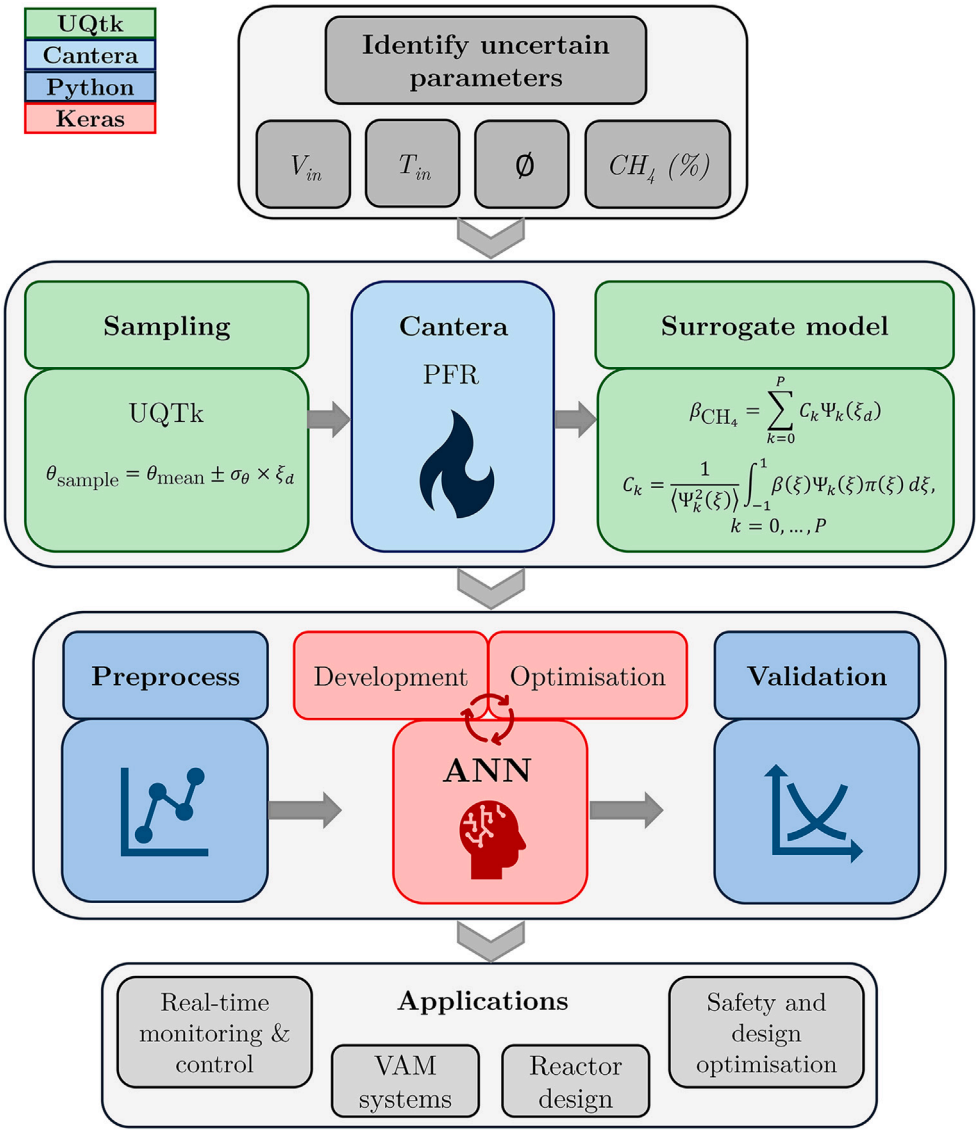

Fig. 3. Overview of the PCE-ANN framework with potential applications.

representing one channel of a honeycomb monolith reactor. A total of 180 cases were investigated, examining four key operational parameters (Table 2): CH_4 concentration in ventilation air (%), T_{in}, V_{in}, and catalyst length (R_c) in mm.

Ultra-lean CH_4 concentrations ranged from 0.2 % to 1.3 % in air, with ± 10 % uncertainty, reflecting varying emission scenarios and corresponding to ϕ of 0.017 to 0.138. Inlet temperatures varied from 800 K to 1000 K (± 2 % uncertainty), as temperature significantly impacts reaction kinetics and catalyst performance. Temperatures below 800 K were avoided due to insufficient O_2 desorption for CH_4 adsorption, while temperatures above 1200 K promote homogeneous CH_4 combustion without a catalyst [9]. Additionally, PtO_2, formed during catalytic oxidation, becomes unstable below 700 K [53], and temperatures above 900 K risk catalyst degradation and thermal NO_x formation. Inlet velocities ranged from 0.8 to 1.2 m/s (± 5 % uncertainty), capturing the effects of flow velocity on CH_4 conversion, residence time, and heat transfer.

The UQ for each case required 216 individual simulations ($(5+1)^3 = 216$), as detailed in Section 2.1, due to the propagation of uncertainties through the system. This resulted in a total of 38,880 data points,

Table 2
Data parameters with applied uncertainty used in ANN algorithm for 1D simulations.

CH_4 (%) ± 10 %					
CH_4 %	Equivalence Ratio (ϕ)				
in the air	Min/max	Mean	T_{in} (K) ± 5 %	V_{in} (m/s) ± 2 %	Catalyst length(mm)
1.3	0.138/0.113	0.125	800–1000	0.8, 1.0, and 1.2	20, 30, and 50
0.9	0.095/0.078	0.086			
0.6	0.063/0.052	0.057			
0.2	0.021/0.017	0.019			

sufficient for training reliable ANN models and accurately quantifying uncertainties.

2.3.2. Model development and optimisation

The relationship between ANN performance and architectural complexity is highly problem-dependent, necessitating a systematic evaluation of various configurations. Prior to ANN training, the input dataset underwent power transformation for normalisation and random shuffling to prevent sequence-based biases. Training employed a batch size of 128, a maximum of 3000 epochs, an initial learning rate of 5×10^{-3} with a decay rate of 1×10^{-4}, and the Adam optimiser with early stopping after 100 consecutive epochs without improvement in the loss function. The Rectified Linear Unit (ReLU) activation function was used across all hidden layers to mitigate gradient vanishing issues. The loss function, mean absolute error (MAE), is defined as:

$$\mathrm{MAE} = \frac{1}{m}\sum_{i=1}^{m} |\mathrm{CH_4}\ \% - \widehat{\mathrm{CH_4}\ \%}| \tag{7}$$

For ANN architecture optimisation, a design space of 2–10 layers and 4–40 neurons per layer was explored, encompassing 81 distinct ANN evaluations. This hyper-parameter optimisation study was completed in approximately 6 hours using an NVIDIA RTX 2000 Ada GPU, demonstrating the efficiency of modern computational resources.

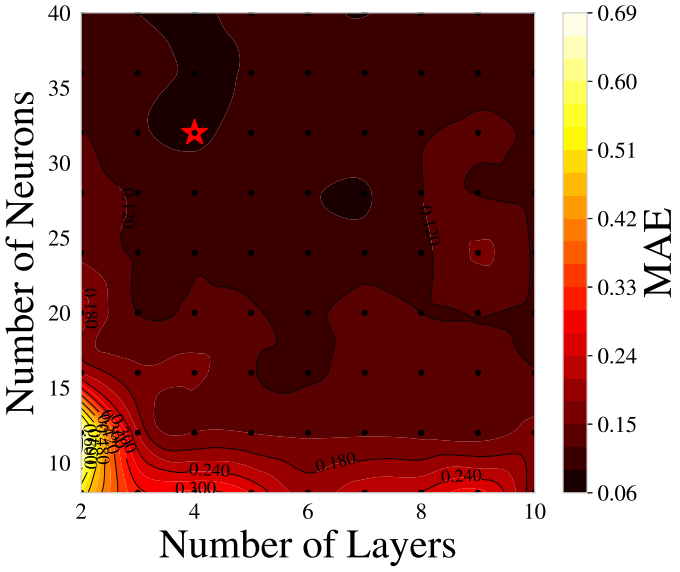

Fig. 4. Accuracy map of ANN architectures in terms of neurons per hidden layer and hidden layers, represented by loss term on the validation set. The red star indicates the lowest MAE, while black circles denote individual ANN evaluations. (For interpretation of the references to colour in this figure legend, the reader is referred to the web version of this article.)

The validation set loss term landscape (Fig. 4) revealed optimal configurations for predictive performance. The lowest MAE values were concentrated in regions with shallow networks (3–5 layers) and 10–15 neurons. The highest accuracy was achieved with a 4-layer, 32-neuron configuration (marked with a red star), chosen for the remainder of this study (Fig. 5).

This architecture achieved an MAE of 0.062 with a minimal generalisation gap between train and validation losses. Networks with increased depth (5–10 layers) maintained stable performance across various neuron counts, suggesting width contributes more significantly to robustness than depth. The steepest error gradients occurred in the lower left corner, where the MAE values rapidly increased to 0.60 and above, indicating inadequate fitting. These findings highlight the importance of systematic hyper-parameter optimisation in ANN design.

To ensure robust model validation, a 5-fold cross-validation strategy was implemented using R^2 scoring Eq. (8) as the evaluation metric on the final model. The cross-validation results demonstrated negligible standard deviation and achieved $\overline{R^2} = 0.995 \pm 0.002$ with $\overline{MAE} = 0.068 \pm 0.013$.

$$R^2 = 1 - \frac{\sum_{i=1}^{m} (CH_4\ \%_i - \widehat{CH_4\ \%_i})^2}{\sum_{i=1}^{m} (CH_4\ \%_i - \overline{CH_4\ \%})^2} \tag{8}$$

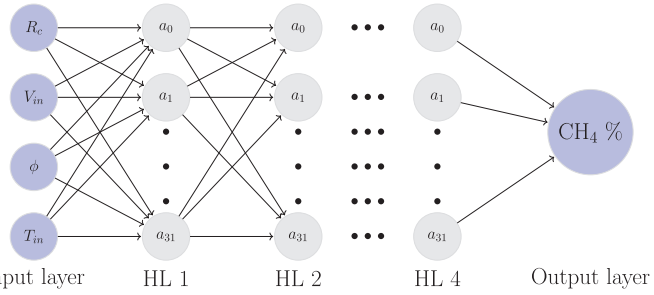

Fig. 5. Schematic of the optimised neural network structure for the given dataset.

The model's predictive accuracy was evaluated by comparing predicted values against ground truth data for the test set (Fig. 6). The comparison plot shows excellent agreement between predictions and actual values across the full range of CH_4 conversion rates (0 %–100 %). Data points closely follow the ideal diagonal line, indicating strong predictive performance. The colour gradient, representing temperature (800–1100 K), demonstrates consistent accuracy across all temperature ranges, with no significant bias or degradation at extremes. The tight clustering of test set predictions along the diagonal confirms the model's ability to generalise to unseen data without overfitting, validating the chosen architecture and training parameters.

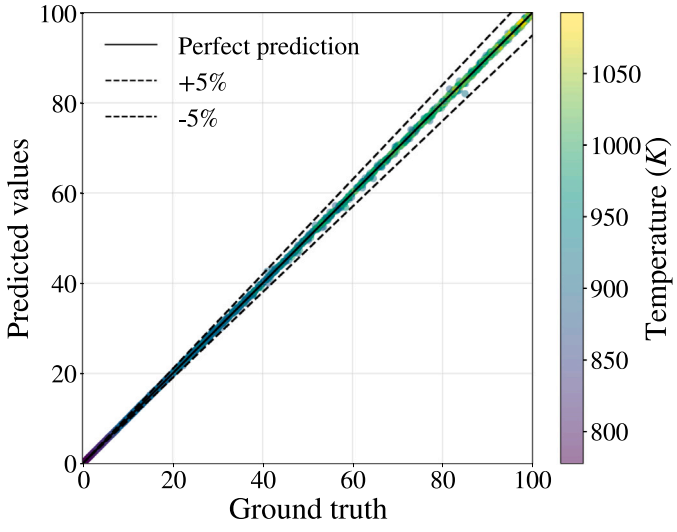

Fig. 6. Ground truth versus predicted values for the test set using the optimal ANN architecture. The dashed lines represent ± 5 % of the ground truth values.

In terms of computational performance, a direct quantitative comparison is not rigorous due to differences in computational resources. Training of the final ML model took around 10 CPU hours on a 13th Gen Intel i7-13850HX CPU. Once trained, the ANN model achieves remarkably fast batch inference, processing the entire training dataset of 38,800 data points in 0.2 s on a single CPU, while data generation required approximately 2500 CPU hours on a high-performance computing cluster.

2.3.3. Model validation

The ML model was validated against 1D Cantera simulations by comparing probability density functions (PDFs) of CH_4 conversion for different operating conditions. The Cantera simulations used a PFR model, which assumes perfect radial mixing and considers axial variations in species concentrations and temperature. This model is suitable for monolithic reactor channels due to their high length-to-diameter ratio and laminar flow conditions. In UQ studies, validating PDF results is critical, as it demonstrates the model's ability to predict the mean values and the complete distribution of outcomes and their likelihood. This is essential for understanding uncertainty propagation and assessing prediction reliability under varying conditions.

Fig. 7 compares PDFs for various inlet velocities (V_{in} = 0.8, 1.0, and 1.2 m/s) and temperatures (850 K to 950 K). The ML model shows excellent agreement with Cantera results across all conditions, accurately capturing both the magnitude and shape of the PDF distributions. This indicates that the ML model has successfully learned the underlying uncertainty propagation mechanisms in the system.

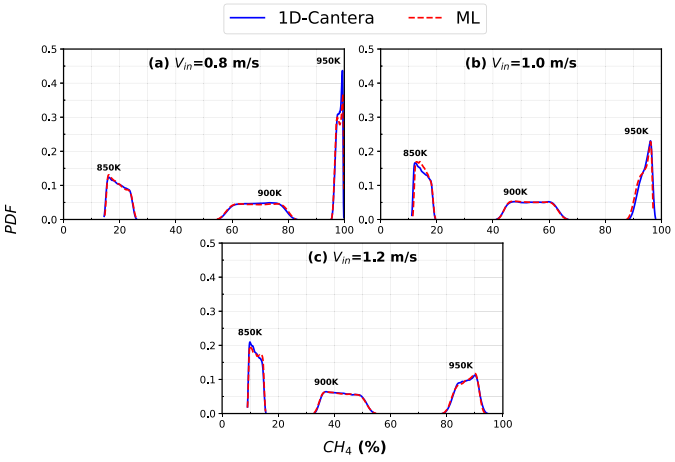

Fig. 7. Validation of CH_4 conversion from Cantera and ML at different T_{in} and V_{in}: **(a)** 0.8 m/s, **(b)** 1.0 m/s, **(c)** 1.2 m/s.

3. Results and discussion

3.1. Effects of CH_4 concentration in air

The effects of CH_4 concentration on the uncertainty in CH_4 conversion were analysed for various T_{in}, with a constant coated channel length of 50 mm and V_{in} of 0.8 m/s. Fig. 8 shows CH_4 conversion as a function of T_{in}, where continuous lines represent mean conversion values, and shaded areas indicate uncertainty bands. Both CH_4 concentration and T_{in} significantly influence the conversion rate and its uncertainty. As concentration increases from 0.6 %–1.3 %, the coefficient of variation (C_V) peaks at approximately 75 % at 850 K for 1.3 % CH_4, indicating higher variability in conversion rates. However, uncertainty decreases significantly at elevated temperatures (>950 K), regardless of CH_4 concentration, demonstrating more stable operations at higher temperatures.

For further insight, Fig. 9 shows PDFs of CH_4 conversion rates at various temperatures and CH_4 concentrations. At lower T_{in} (850 K), PDFs for higher CH_4 concentrations exhibit wider distributions, consistent with the uncertainty bands in Fig. 8. As T_{in} increases, PDFs for higher CH_4 concentrations become narrower and sharply peaked in the high conversion region (80 %–100 %), supporting the stability of CH_4 conversion at elevated temperatures.

3.2. Effects of inlet velocity (V_{in})

Inlet velocity, which controls ventilation airflow, is critical for safety and emission control in industrial settings. Higher ventilation rates

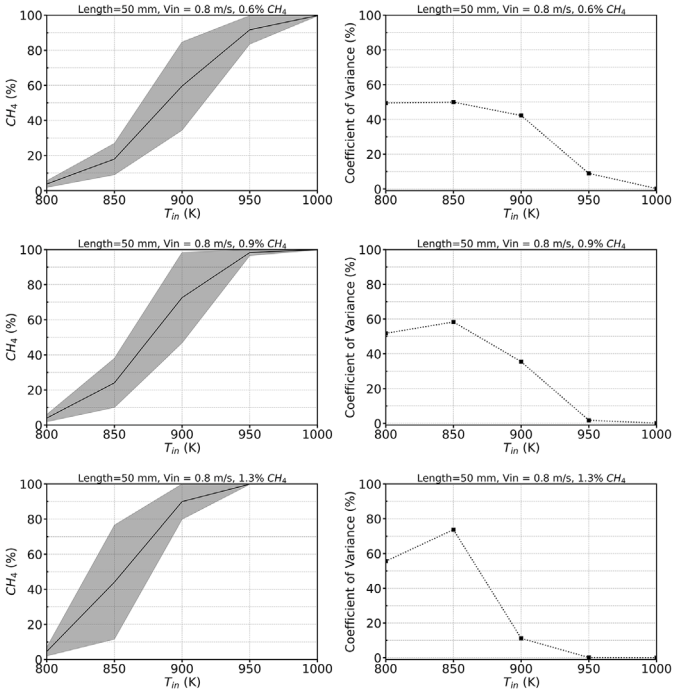

Fig. 8. Effect of uncertainty on CH_4 conversion for different inlet temperatures. Continuous lines represent the mean conversion values, while shaded areas indicate the uncertainty bands due to the deviations in input parameters.

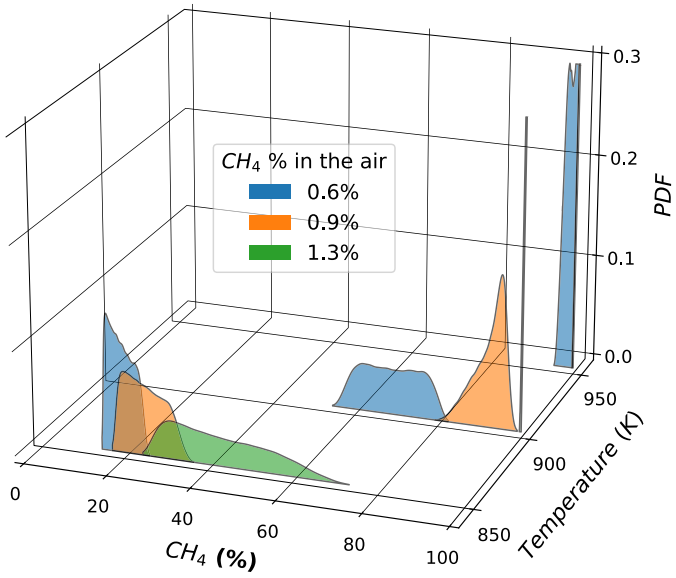

Fig. 9. PDFs for different CH_4 concentrations in air at various temperatures.

ensure safer conditions by diluting CH_4 below explosive limits but reduce catalytic conversion efficiency by decreasing residence time. The effect of V_{in} on CH_4 conversion uncertainty was analysed for three velocities (0.8, 1.0, and 1.2 m/s) at a constant CH_4 concentration of 0.6 % and a catalyst-coated channel length of 50 mm. Fig. 10 shows that CH_4 conversion rates are consistently higher at lower V_{in}, attributed to increased residence time. While C_V values are similar (around 50 %) at 800 K, they diverge with increasing T_{in}. For V_{in} = 0.8 m/s, C_V decreases rapidly to 10 % at 950 K, whereas higher V_{in} (1.0 and 1.2 m/s) show slower decreases, reaching 17 % and 22 %, respectively. These results highlight

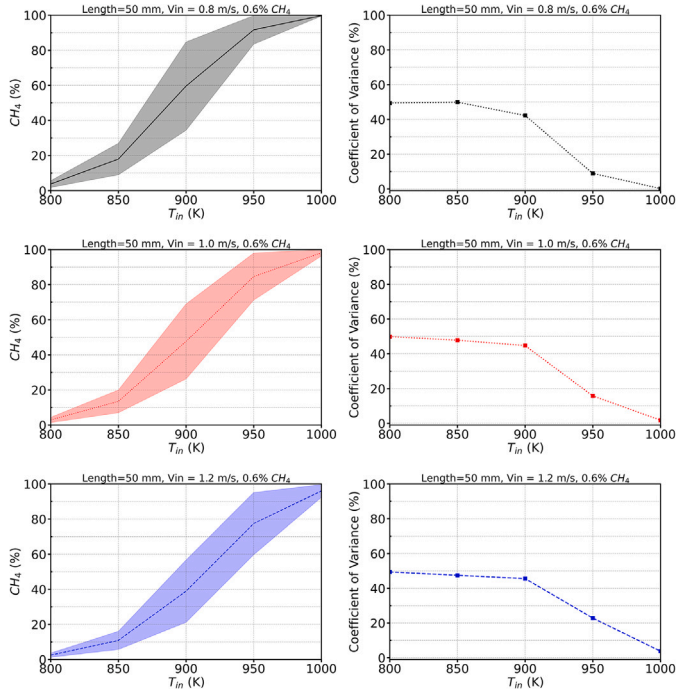

Fig. 10. Comparison of uncertainty effects on CH_4 conversion for 0.6 % CH_4 in air at different inlet velocities. Continuous lines represent the mean conversion values, while shaded areas indicate the uncertainty bands due to the deviations in input parameters.

the trade-off between safety and conversion efficiency, emphasising the need to optimise operating temperatures based on ventilation rates.

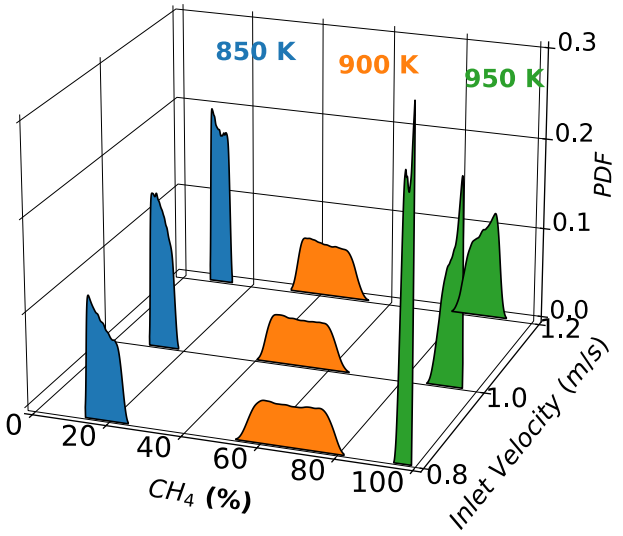

Fig. 11. PDF comparison of CH_4 conversion for different T_{in} and V_{in} for a 50 mm catalyst-coated reactor with 0.6 % CH_4 in air.

For further analysis, Fig. 11 shows PDFs of CH_4 conversion at different V_{in} and T_{in} for a 50 mm catalyst-coated reactor with 0.6 % CH_4 in air. At 950 K, CH_4 conversion exhibits reduced uncertainty with narrower PDFs at lower V_{in}. However, at 900 K, PDFs are wider and less stable regardless of V_{in}, highlighting the importance of temperature control in achieving consistent conversion rates.

3.3. Effect of inlet temperature (T_{in})

Inlet temperature plays a crucial role in CH_4 conversion, as higher temperatures enhance catalyst activity, promoting more complete conversion. Fig. 12 shows the effects of T_{in} on CH_4 conversion rates and their associated uncertainties for different CH_4 concentrations. At lower T_{in} (850 K), CH_4 conversion rates are low due to limited catalytic activity, increasing gradually from 15 % at 0.2 % CH_4 to 45 % at 1.3 % CH_4. Uncertainty also increases with T_{in}, peaking at 75 % for 1.3 % CH_4, consistent with the discussion in Section 3.1. At higher T_{in} (>900 K), C_V decreases with CH_4 concentration, indicating more stable conversion. For T_{in} = 950 K, CH_4 conversion rates reach 60 %–100 %, with complete conversion at 1.3 % CH_4, demonstrating that elevated temperatures enhance both conversion rates and process stability.

While V_{in} affects CH_4 conversion uncertainty by influencing residence time, T_{in} has a more fundamental impact. Fig. 13 shows the main sensitivity analysis for various T_{in} and CH_4 concentrations (0.2 %–1.3 %) at different V_{in}. T_{in} is the primary contributor to uncertainty, especially at lower T_{in} and CH_4 concentrations. Its contribution decreases with increasing T_{in} and CH_4 concentration, while the impact of CH_4 concentration (ϕ) and V_{in} becomes more significant. At higher T_{in} (950 K) and CH_4 concentrations, the order of contribution to uncertainty is $T_{in} > \phi > V_{in}$, highlighting the importance of temperature control for stability at lower equivalence ratios and flow velocities.

3.4. Effects of catalyst coating length

Catalyst deactivation is a significant challenge in real catalytic CH_4 conversion reactors, particularly in systems processing low-concentration CH_4 in air, which often contains contaminants such as dust, NO_x, H_2O, H_2S, and SO_2. These impurities can degrade catalyst performance or cause complete deactivation [9]. To understand the impact of deactivation, three catalyst coating lengths (50, 30, and 20 mm) were analysed, representing varying stages of catalyst availability. These reduced coating lengths serve as a simplified representation of the effective active catalyst area remaining after partial deactivation. While this approach does not capture the full complexity of deactivation dynamics, it provides valuable insights into how reduced catalyst availability affects both conversion efficiency and process predictability. Fig. 14 shows that shorter coating lengths lead to lower CH_4 conversion rates and higher uncertainty. C_V values decrease with increasing T_{in}, but this decrease is less pronounced for shorter coating lengths, indicating that

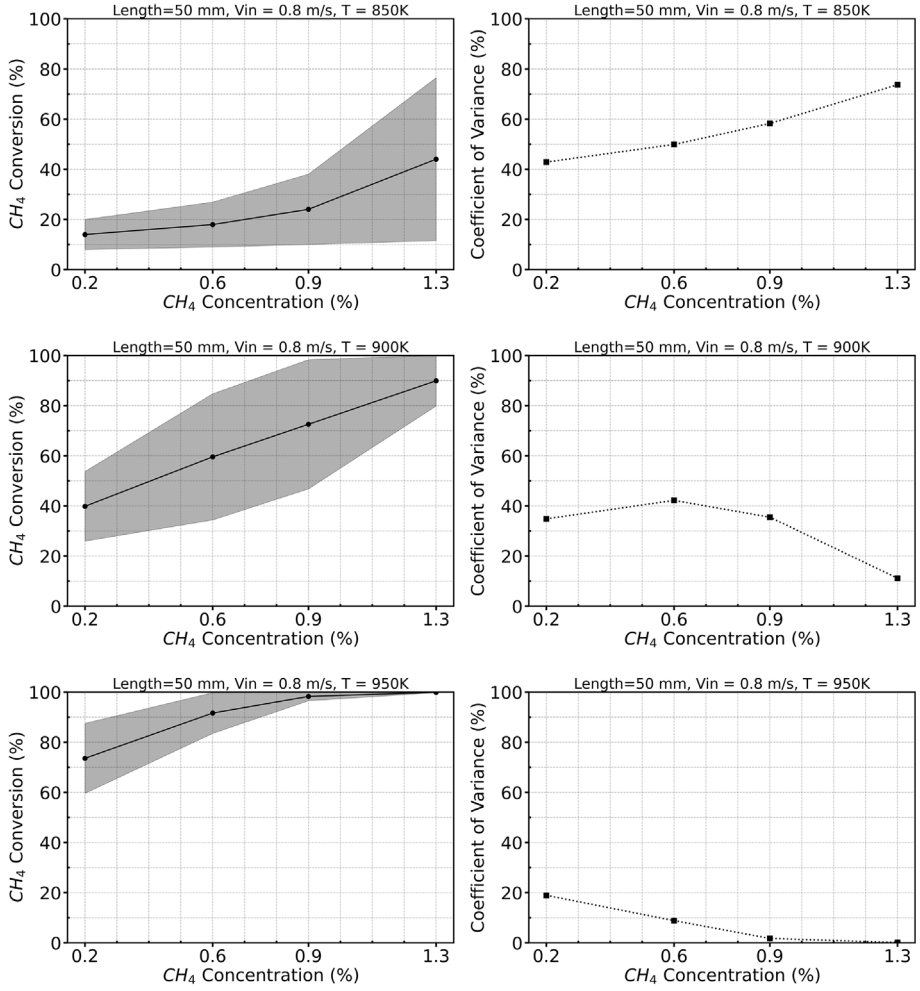

Fig. 12. Effect of uncertainty on CH_4 conversion for different CH_4 concentrations in air at various temperatures. Continuous lines represent the mean conversion values, while shaded areas indicate the uncertainty bands due to the deviations in input parameters.

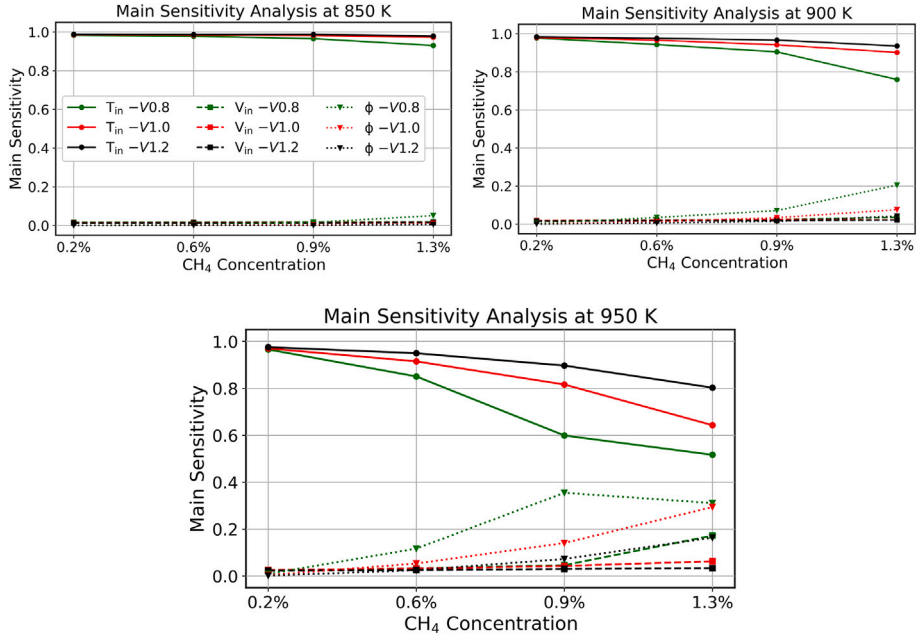

Fig. 13. Main sensitivity analysis at various T_{in} and CH_4 concentrations for different inlet velocities.

catalyst deactivation reduces both conversion efficiency and process predictability.

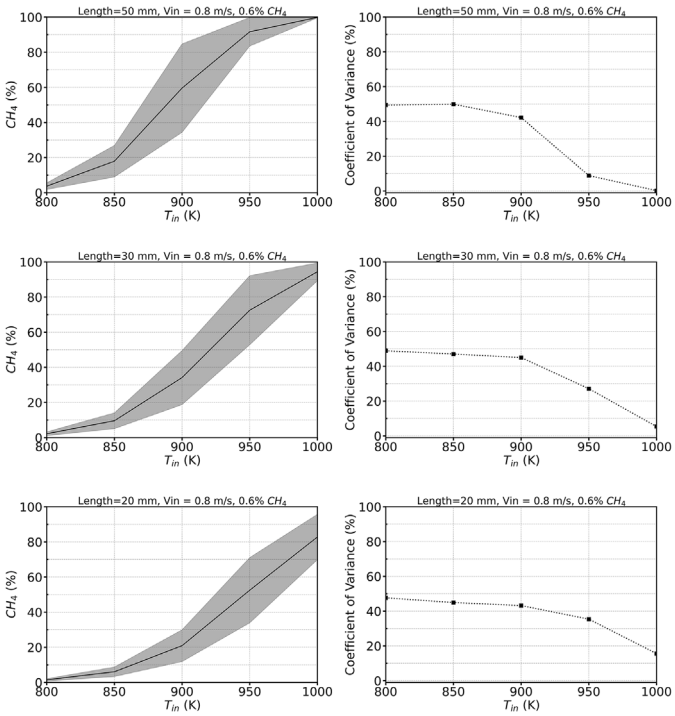

Fig. 14. Effect of catalyst coating length in the monolith channel on CH_4 conversion rate and uncertainty. Continuous lines represent the mean conversion values, while shaded areas indicate the uncertainty bands due to the deviations in input parameters.

Specifically, at T_{in} = 850 K, reducing coating length from 50 mm to 20 mm decreases mean CH_4 conversion from approximately 20 % to 10 %, while C_V decreases from 50 % to 45 %. The more dramatic effect is seen at higher temperatures (T_{in} = 950 K), conversion drops from nearly 100 % to 60 %, demonstrating that deactivation has greater absolute impact at conditions where the fresh catalyst would otherwise achieve complete conversion. Critically, the uncertainty (C_V) remains elevated even at high temperatures when catalyst is deactivated. For the 50 mm coating, C_V drops to 5 % at 950 K, indicating very stable conversion performance. However, for the 20 mm coating, which represents around 60 % deactivation, C_V remains at 35 % even at 950 K. This persistent uncertainty under deactivated conditions has important implications: operators cannot compensate for deactivation simply by increasing temperature, as the system becomes inherently less predictable and more sensitive to input variations.

It should be noted that the representation of deactivation solely by reduction in coating length is a simplification of the complex deactivation phenomena occurring in real systems. In practice, catalyst deactivation can occur through multiple mechanisms, including poisoning by sulphur compounds, H_2O vapour, sintering at higher temperatures, and fouling by dust particles, which may alter not only the available surface area but also the intrinsic catalytic activity of remaining sites. The current simplified model assumes that the remaining catalyst maintains its original activity while the "deactivated" region has zero activity, which may not fully capture scenarios where poisoning or sintering reduce the intrinsic activity across the entire catalyst bed. Despite these limitations, this approach provides valuable first-order insights into how reduced catalyst availability affects conversion performance and uncertainty propagation, with the key finding that deactivation increases conversion uncertainty expected to be robust regardless of the specific deactivation mechanism.

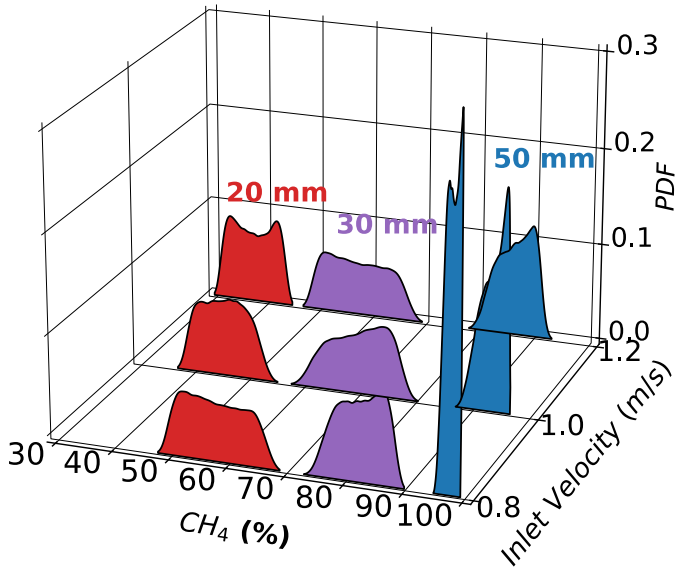

Fig. 15. PDF comparison of CH_4 conversion at different V_{in} for various catalyst coating lengths at 950 K and 0.6% CH_4 concentration in air.

For further illustration, Fig. 15 shows PDFs of CH_4 conversion at 950 K for 0.6 % CH_4 in air, comparing different V_{in} and catalyst coating lengths. Longer coating lengths result in higher conversion rates and more stable performance, evidenced by narrow, sharply peaked PDFs centred at high conversion values. For V_{in} = 0.8 m/s with 50 mm coating, the PDF shows a sharp peak at 95 % conversion with minimal spread, indicating consistent, reliable performance. In contrast, the 20 mm coating produces a broader PDF centred at around 75 % conversion, with significant probability mass between 60 %–85 %. This wider distribution indicates that under identical operating conditions, the partially deactivated catalyst produces highly variable outcomes, sometimes achieving acceptable conversion, other times falling well below target performance. This effect is more pronounced at higher V_{in} (1.2 m/s), where the reduced residence time exacerbates the impact of deactivation. The 20 mm coating at high velocity produces the broadest PDF, spanning 40 %–70 % conversion, making performance prediction difficult and control strategy implementation challenging. These results highlight that catalyst deactivation not only reduces mean CH_4 conversion rates but also fundamentally alters the system's uncertainty characteristics, increasing operational risk and reducing process reliability. For V_{in} = 0.8 m/s, shorter coatings result in broader PDFs with lower peak heights, indicating less stable and lower conversion outcomes. This effect is more pronounced at higher V_{in}, aligning with the analysis in Section 3.2. These results highlight that catalyst deactivation not only reduces CH_4 conversion rates but also increases uncertainty, emphasising the need for regular monitoring and maintenance, especially at higher flow rates.

4. Conclusions

In this work, the effects of variability in ultra-lean fugitive methane combustion were investigated for various CH_4 concentrations ranging from 0.2 % to 1.3 % in air with ±10 % uncertainty, corresponding to equivalence ratios (ϕ) between 0.017 and 0.138. Additionally, variations in inlet temperatures from 800 K to 1000 K (±2 % uncertainty) and inlet velocities from 0.8 to 1.2 m/s (±5 % uncertainty) were analysed for various catalyst lengths (20, 30, and 50 mm). The study employed the validated Deutschmann et al. [18] mechanism to simulate a PFR model for 1D catalytic CH_4 combustion over a Pt catalyst. For the first time, a data-driven PCE-based UQ method was applied to investigate the impact of small parameter variations on CH_4 conversion in a PFR, representing a

single channel of a honeycomb reactor. Additionally, catalytic CH_4 conversion, along with associated uncertainty, was successfully modelled and predicted using an ML approach via an ANN.

Key findings from this study are as follows:

- The ANN model not only showed excellent agreement with 1D PFR simulations under various conditions but also demonstrated strong agreement with probability distributions arising from parameter uncertainties while reducing computational time from hours to mere seconds.
- Uncertainty in catalytic CH_4 conversion increases with fugitive CH_4 concentration in air, with a C_V reaching 75 % for a 1.3 % CH_4 concentration at $T_{in} = 850$ K.
- The uncertainty effect diminishes significantly as T_{in} increases, particularly for $T_{in} > 950$ K, where the catalytic process becomes more stable regardless of methane concentration.
- Catalytic CH_4 conversion is more stable at lower velocities, with C_V rapidly decreasing to about 10 % at 950 K, whereas at higher velocities, C_V remains in the range of 17 %–22 % under the same conditions.
- CH_4 conversion rate decreases while uncertainty increases as the catalyst-coated channel length decreases across all operating temperatures. This effect is more pronounced at higher flow velocities.
- Inlet temperature emerged as the dominant factor affecting uncertainty, irrespective of other parameters.

These findings underscore the crucial role of temperature control and regular catalyst maintenance, particularly when higher ventilation rates are required for safety. Overall, parameter variations can induce up to 75 % uncertainty in catalytic CH_4 conversion rates. It is important to note that the PCE-ANN framework is fuel- and reactor-agnostic, offering a versatile computational tool applicable to a wide range of catalytic processes where UQ is critical for robust system design and operation. Future investigations could focus on exploring different catalyst materials and their influence on UQ, assessing the impact of trace impurities such as dust, NO_x, H_2O, and common poisons (e.g., H_2S, SO_2) on conversion rate uncertainty and system reliability, and developing more comprehensive models to simulate catalyst deactivation and transient operating conditions typical of VAM systems. Additionally, evaluating the framework's ability to generalise across channel geometries and validating these simulations experimentally would provide valuable insights into the practical implications of UQ in catalytic methane combustion.

CRediT authorship contribution statement

Israfil Soyler: Writing – original draft, Validation, Software, Methodology, Investigation, Formal analysis, Data curation. **Cihat Emre Üstün:** Writing – review & editing, Visualization, Software, Methodology, Data curation. **Amin Paykani:** Writing – review & editing, Conceptualization. **Xi Jiang:** Writing – review & editing. **Nader Karimi:** Writing – review & editing, Supervision, Funding acquisition, Data curation, Conceptualization.

Declaration

During the preparation of this work the authors used ChatGPT in order to improve the clarity of text in some parts of the manuscript. After using this service, the authors reviewed and edited the content as needed and take full responsibility for the content of the publication.

Declaration of competing interest

The authors declare that they have no known competing financial interests or personal relationships that could have appeared to influence the work reported in this paper.

Acknowledgements

Israfil Soyler acknowledges the Republic of Türkiye Ministry of National Education for their financial support through a PhD scholarship. N. Karimi acknowledges the financial support provided by EPSRC through grant number EP/X019551/1.

Data availability

Data will be made available on request.

References

[1] IPCC. Climate change 2007, Available online (2008). https://www.ipcc.ch/site/assets/uploads/2018/05/ar4-wg1-errata.pdf [accessed: November 10, 2025].
[2] International Energy Agency. World energy outlook 2024, Report, Paris, license: Report: CC BY 4.0; Annex A: CC BY NC SA 4.0 IEA; 2024.
[3] International Energy Agency. Global methane tracker 2024, Report, Paris, licence: CC BY 4.0 IEA; 2024. https://www.iea.org/reports/global-methane-tracker-2024.
[4] United Nations Publications. Best practice guidance for effective methane drainage and use in coal mines, ECE energy series. United Nations Economic Commission for Europe; 2016. https://books.google.com.tr/books?id=HfwEDcx6K3YC.
[5] Yang Z, Hussain MZ, Marchín P, Jia Q, Wang N, Ordóñez S, Zhu Y, Xia Y. Enrichment of low concentration methane: an overview of ventilation air methane. J Mater Chem A 2022;10(12):6397–413.
[6] Lee JH, Trimm DL. Catalytic combustion of methane. Fuel Process Technol 1995;42(2–3):339–59.
[7] Setiawan A, Kennedy EM, Stockenhuber M. Development of combustion technology for methane emitted from coal-mine ventilation air systems. Energy Technol 2017;5(4):521–38.
[8] Sharma HN, Sharma V, Mhadeshwar AB, Ramprasad R. Why pt survives but pd suffers from so x poisoning? J Phys Chem Lett 2015;6(7):1140–8.
[9] Feng X, Jiang L, Li D, Tian S, Zhu X, Wang H, He C, Li K. Progress and key challenges in catalytic combustion of lean methane. J Energy Chem 2022;75:173–215.
[10] Su S, Yu X. A 25ákwe low concentration methane catalytic combustion gas turbine prototype unit. Energy 2015;79:428–38.
[11] Burch R, Loader PK. Investigation of pt/al2o3 and pd/al2o3 catalysts for the combustion of methane at low concentrations. Appl Catal B Environ 1994;5(1–2):149–64.
[12] Wei X, Kang J, Gan L, Wang W, Yang L, Wang D, Zhong R, Qi J. Recent advances in co3o4-based composites: synthesis and application in combustion of methane. Nanomaterials 2023;13(13):1917. https://doi.org/10.3390/nano13131917
[13] Xu X, Liu W, Liu H, Li Y, Gao X, Lu B, Qi J, Li Z, Han J, Yan Y. Self-supporting characteristics in hierarchical monolith catalyst with highly accessible active sites for boosting lean methane catalytic oxidation. Fuel 2026;405:136576. https://doi.org/10.1016/j.fuel.2025.136576
[14] He L, Fan Y, Bellettre J, Yue J, Luo L. Catalytic methane combustion in plate-type microreactors with different channel configurations: an experimental study. Chem Eng Sci 2021;236:116517.
[15] Hunt G, Karimi N, Mehdizadeh A. Intensification of ultra-lean catalytic combustion of methane in microreactors by boundary layer interruptions–a computational study. Chem Eng Sci 2021;242:116730.
[16] Dupont V, Moallemi F, Williams A, Zhang S-H. Combustion of methane in catalytic honeycomb monolith burners. Int J Energy Res 2000;24(13):1181–201.
[17] Kumaresh S, Kim MY. Numerical investigation of catalytic combustion in a honeycomb monolith with lean methane and air premixtures over the platinum catalyst. Int J Therm Sci 2019;138:304–13.
[18] Deutschmann O, Behrendt F, Warnatz J. Modelling and simulation of heterogeneous oxidation of methane on a platinum foil. Catal Today 1994;21(2–3):461–70.
[19] Jiang X, Mira D, Cluff DL. The combustion mitigation of methane as a non-co2 greenhouse gas. Prog Energy Combust Sci 2018;66:176–99.
[20] Rahimi S, Ataee-Pour M, Madani H, Aminossadati SM. Investigating the impact of gas emission uncertainty on airflow distribution in an auxiliary ventilation system using cfd and monte-carlo simulation. Build Environ 2021;204:108165.
[21] He L, Fan Y, Bellettre J, Yue J, Luo L. A review on catalytic methane combustion at low temperatures: catalysts, mechanisms, reaction conditions and reactor designs. Renew Sustain Energy Rev 2020;119:109589.
[22] Thevenin PO, Ersson AG, Kušar HMJ, Menon PG, Järås SG. Deactivation of high temperature combustion catalysts. Appl Catal A Gen 2001;212(1–2):189–97.
[23] Ozcan H, Kayabasi E. Thermodynamic and economic analysis of a synthetic fuel production plant via co2 hydrogenation using waste heat from an iron-steel facility. Energy Convers Manag 2021;236:114074.
[24] Wang H. Uncertainty quantification and minimization. In: Computer aided chemical engineering, vol. 45: Elsevier; 2019. pp. 723–62.
[25] Helton JC, Johnson JD, Oberkampf WL, Sallaberry CJ. Representation of analysis results involving aleatory and epistemic uncertainty. Int J Gen Syst 2010;39(6):605–46.
[26] Wang H, Sheen DA. Combustion kinetic model uncertainty quantification, propagation and minimization. Prog Energy Combust Sci 2015;47:1–31.
[27] Turányi T, Nagy T, Zsély IG, Cserháti M, Varga T, Szabó BT, Sedyo I, Kiss PT, Zempleni A, Curran HJ. Determination of rate parameters based on both direct and indirect measurements. Int J Chem Kinet 2012;44(5):284–302.
[28] Knio OM, Najm HN, Ghanem RG, et al. A stochastic projection method for fluid flow: I. basic formulation. J Comput Phys 2001;173(2):481–511.

[29] Tripathy R, Bilionis I, Gonzalez M. Gaussian processes with built-in dimensionality reduction: applications to high-dimensional uncertainty propagation. J Comput Phys 2016;321:191–223.
[30] Üstün CE, Paykani A. Probabilistic machine learning framework for chemical source term integration with gaussian processes: H2/air auto-ignition case. Int J Hydrogen Energy 2024;81:47–55.
[31] Zhang K, Jiang X. An investigation of fuel variability effect on bio-syngas combustion using uncertainty quantification. Fuel 2018;220:283–95.
[32] Najm HN. Uncertainty quantification and polynomial chaos techniques in computational fluid dynamics. Annu Rev Fluid Mech 2009;41(1):35–52.
[33] Najm HN, Debusschere BJ, Marzouk YM, Widmer S, Le Maître OP. Uncertainty quantification in chemical systems. Int J Numer Methods Eng 2009;80(6–7):789–814.
[34] Reagan MT, Najm HN, Pébay PP, Knio OM, Ghanem RG. Quantifying uncertainty in chemical systems modeling. Int J Chem Kinet 2005;37(6):368–82.
[35] Tang Y, Hassanaly M, Raman V, Sforzo B, Seitzman J. A comprehensive modeling procedure for estimating statistical properties of forced ignition. Combustion And Flame 2019;206:158–76.
[36] Soyler I, Zhang K, Duwig C, Jiang X, Karimi N. Uncertainty quantification of the premixed combustion characteristics of nh3/h2/n2 fuel blends. Int J Hydrogen Energy 2023;48(38):14477–91.
[37] Soyler I, Zhang K, Jiang X, Karimi N. Effects of compositional uncertainties in cracked nh3/biosyngas fuel blends on the combustion characteristics and performance of a combined-cycle gas turbine: a numerical thermokinetic study. Int J Hydrogen Energy 2024;69:504–17.
[38] Zhang K, Jiang X. Uncertainty quantification of fuel variability effects on high hydrogen content syngas combustion. Fuel 2019;257:116111.
[39] Zhang K, Jiang X. An assessment of fuel variability effect on biogas-hydrogen combustion using uncertainty quantification. Int J Hydrogen Energy 2018;43(27):12499–515.
[40] Anwar M, Soyler I, Karimi N. Machine learning-enhanced uncertainty quantification for renewable-powered hybrid green ammonia and refrigeration systems: Technoeconomic and environmental effects. J Clean Prod 2025;527:146702. https://doi.org/10.1016/j.jclepro.2025.146702.
[41] Üstün CE, Herfatmanesh MR, Valera-Medina A, Paykani A. Applying machine learning techniques to predict laminar burning velocity for ammonia/hydrogen/air mixtures. Energy And AI 2023;13:100270.
[42] Üstün CE, Eckart S, Valera-Medina A, Paykani A. Data-driven prediction of laminar burning velocity for ternary ammonia/hydrogen/methane/air premixed flames. Fuel 2024;368:131581.
[43] Cui Y, Wang Q, Liu H, Zheng Z, Wang H, Yue Z, Yao M. Development of the ignition delay prediction model of n-butane/hydrogen mixtures based on artificial neural network. Energy And AI 2020;2:100033.
[44] Alotaibi FN, Berrouk AS, Saeed M. Optimization of yield and conversion rates in methane dry reforming using artificial neural networks and the multiobjective genetic algorithm. Ind Eng Chem Res 2023;62(42):17084–99.
[45] Zhou L, Song Y, Ji W, Wei H. Machine learning for combustion. Energy And AI 2022;7:100128.
[46] Debusschere B, Sargsyan K, Safta C, Chowdhary K. The uncertainty quantification toolkit (uqtk). In Ghanem R, Higdon D, Owhadi H, editors. Handbook of uncertainty quantification. Springer; 2017. pp. 1807–27. http://www.springer.com/us/book/9783319123844.
[47] Xiu D, Karniadakis GE. The wiener–askey polynomial chaos for stochastic differential equations. SIAM J Sci Comput 2002;24(2):619–44.
[48] Xiong F, Chen S, Xiong Y. Dynamic system uncertainty propagation using polynomial chaos. Chin J Aeronaut 2014;27(5):1156–70.
[49] Kucherenko S, Song S. Different numerical estimators for main effect global sensitivity indices. Reliab Eng Syst Saf 2017;165:222–38.
[50] Deutschmann O, Maier LI, Riedel U, Stroemman AH, Dibble RW. Hydrogen assisted catalytic combustion of methane on platinum. Catal. Today 2000;59(1–2):141–50.
[51] Goodwin DG, Moffat HK, Speth RL. Cantera: an object-oriented software toolkit for chemical kinetics, thermodynamics, and transport processes. Zenodo 2018.
[52] Cornejo I, Nikrityuk P, Hayes RE. Heat and mass transfer inside of a monolith honeycomb: from channel to full size reactor scale. Catal. Today 2022;383:110–22.
[53] Gélin P, Primet M. Complete oxidation of methane at low temperature over noble metal based catalysts: a review. Appl Catal B Environ 2002;39(1):1–37.